Separation Science and Technology
Publication details, including instructions for authors and subscription information:
http://www.informaworld.com/smpp/title~content=t713708471

Single and Multicomponent Sorption of CO_2, CH_4 and N_2 in a Microporous Metal-Organic Framework

Patrick S. Bárcia[a]; Laurent Bastin[a]; Eric J. Hurtado[b]; José A. C. Silva[a]; Alírio E. Rodrigues[c]; Banglin Chen[b]
[a] Escola Superior de Tecnologia e Gestão, Instituto Politécnico de Bragança, Bragança, Portugal [b] Department of Chemistry, University of Texas-Pan American, Edinburg, TX, USA [c] Laboratory of Separation and Reaction Engineering, Departamento de Engenharia Química, Faculdade de Engenharia, Universidade do Porto, Porto, Portugal

To cite this Article Bárcia, Patrick S. , Bastin, Laurent , Hurtado, Eric J. , Silva, José A. C. , Rodrigues, Alírio E. and Chen, Banglin(2008) 'Single and Multicomponent Sorption of CO_2, CH_4 and N_2 in a Microporous Metal-Organic Framework', Separation Science and Technology, 43: 13, 3494 — 3521
To link to this Article: DOI: 10.1080/01496390802282347
URL: http://dx.doi.org/10.1080/01496390802282347

Separation Science and Technology, 43: 3494–3521, 2008

ISSN: 0149-6395 print/1520-5754 online
DOI: 10.1080/01496390802282347

Taylor & Francis
Taylor & Francis Group

Single and Multicomponent Sorption of CO_2, CH_4 and N_2 in a Microporous Metal-Organic Framework

Patrick S. Bárcia,[1] Laurent Bastin,[1] Eric J. Hurtado,[2] José A. C. Silva,[1] Alírio E. Rodrigues,[3] and Banglin Chen[2]

[1]Escola Superior de Tecnologia e Gestão, Instituto Politécnico de Bragança, Bragança, Portugal

[2]Department of Chemistry, University of Texas-Pan American, Edinburg, TX, USA

[3]Laboratory of Separation and Reaction Engineering, Departamento de Engenharia Química, Faculdade de Engenharia, Universidade do Porto, Porto, Portugal

Abstract: Single and multicomponent fixed-bed adsorption of CO_2, N_2, and CH_4 on crystals of MOF-508b has been studied in this work. Adsorption equilibrium was measured at temperatures ranging from 303 to 343 K and partial pressures up to 4.5 bar. MOF-508b is very selective for CO_2 and the loadings of CH_4 and N_2 are practically temperature independent. The Langmuir isotherm model provides a good representation of the equilibrium data. A dynamic model based on the LDF approximation for the mass transfer has been used to describe with good accuracy the adsorption kinetics of single, binary and ternary breakthrough curves. It was found that the intra-crystalline diffusivity for CO_2 is one order of magnitude faster than for CH_4 and N_2.

Keywords: CO_2 separation, dynamic simulation, fixed bed, dynamic, metal-organic framework, multi-component adsorption, natural gas

Received 4 March 2008; accepted 19 May 2008.

Address correspondence to Alírio E. Rodrigues, Laboratory of Separation and Reaction Engineering (LSRE), Department of Chemical Engineering, Faculty of Engineering, University of Porto, Rua Dr. Roberto Frias s/n, Porto, 4200-465 Portugal. Tel.: 351 22 508167; Fax: 351 22 5081674. E-mail: arodrig@fe.up.pt

INTRODUCTION

The quality of natural gas can vary widely according to the location of the plant; nevertheless its composition can include up to 10% and 5% of carbon dioxide (CO_2) and nitrogen (N_2), respectively. Natural gas containing high levels of CO_2 and N_2 represent approximately one-third of the U.S. natural gas resource (1). In many cases, this *low quality gas* cannot be treated from the economic point of view with existing processing technology, which means that huge amounts of fuel remain underground (2). The continuous exhaustion of the producing wells, added to the fact that unexploited reserves contain higher fractions of low quality gas will stress the need for more efficient purifying processes able to meet the quality standards specified by the major pipeline transmission and distribution companies.

At the same time, a novel class of crystalline microporous adsorbents has found great interest; the metal-organic frameworks (MOFs) have the potential for making a significant impact in separation processes since they offer the possibility to be tuned varying their pore size and functionality for specific applications. In a recent article (3), we have presented a sorption equilibrium study for the adsorption of CO_2, CH_4, and N_2 in a microporous MOF Zn(BDC)(4,4′-Bipy)$_{0.5}$ (MOF-508b) (4,4′-Bipy = 4,4′-bipyridine) (4) with one-dimensional pores of about 4.0×4.0 Å (See Fig. 1). It was referred to by Bastin et al. (3) that the significant difference in the quadrupole moment of these molecules plays an important role resulting in the preferential adsorption of CO_2, relatively to CH_4 and N_2.

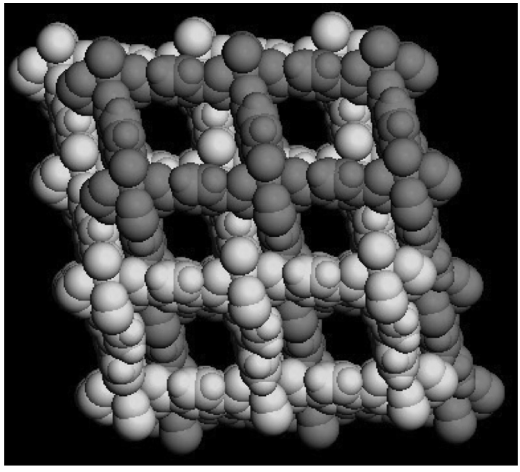

Figure 1. One-dimensional micropores of about 4.0×4.0 Å in 4 MOF-508b.

In this work, we will present the first example of mathematical modeling for fixed-bed adsorption of gas mixtures in microporous MOFs. Sorption equilibrium data of CO_2, CH_4, and N_2 in MOF-508b at 303, 323, and 343 K and partial pressures up to 4.5 bar are reported for the three gases. These data are fitted with a simple Langmuir isotherm model, the results being presented in several figures along the article. Single, binary, and ternary breakthrough curves were measured to provide required data to develop and validate a model based on the LDF approximation for the mass transfer, which could be used in the implementation of an adsorption processes for the purification of the natural gas.

EXPERIMENTAL SECTION

Adsorbates and Adsorbent

The adsorbates under investigation were CO_2, CH_4 and N_2. All the gases containing purity higher than 99.5% were supplied by Air Liquide. Physical properties of these gases are summarized in Table 1.

The microporous MOF-508b Zn(BDC)(4,4′-Bipy)$_{0.5}$ (**1**) (4,4′-Bipy = 4,4′-bipyridine) was synthesized according to the procedure in ref. (4).

Equipment and Procedure

Adsorption equilibrium data were obtained from breakthrough experiments in a laboratorial unit existing at LSRE. Figure 2 shows a schematic representation of the apparatus used to measure single and multicomponent breakthrough curves. A detailed description of the apparatus set-up is given in a previous work (3).

The experimental procedure follows: An adsorption column packed with crystals of MOF-508b dispersed in glass wool was operated by introducing a constant flowrate of the adsorbate gas mixture with known

Table 1. Adsorbate properties (21,22)

Physical property	CO_2	N_2	CH_4
Kinetic diameter (Å)	3.30	3.64	3.80
Dipole moment $\times 10^{18}$ (esu cm)	0	0	0
Quadrupole moment $\times 10^{26}$ (esu cm^2)	4.30	1.52	0
Polarizability $\times 10^{25}$ (cm^3)	31.0	17.6	26.0

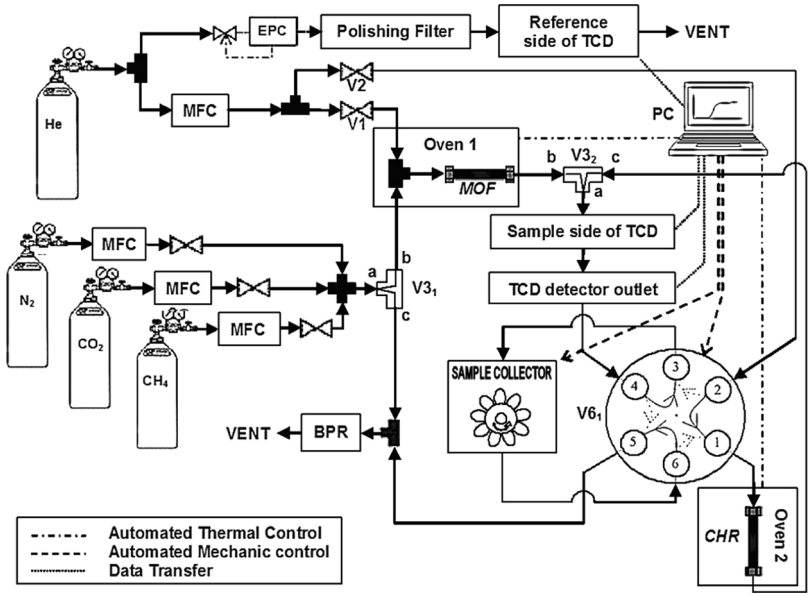

Figure 2. Schematic diagram of the apparatus used to measure adsorption equilibrium for mono- and multi-component systems: (BPR) back pressure regulator; (Sample collector) 10 sample-loops; (CHR) chromatographic silica gel column; (MOF) packed column containing MOF; (EPC) electronic pressure controller; (MFC) mass flow controller; (PC) Computer; (TCD) thermal conductivity detector; (V_1, V_2) valves; ($V3_1$, $V3_2$) 3-ways valves; (V6) 6-ways crossover valve; (①,②,③,④,⑤,⑥) streams.

composition in a helium stream at a fixed total pressure. The analysis of the system consists in measuring continuously the mass flow at the outlet of the packed bed with a thermal conductivity detector (TCD). In multicomponent experiments, samples are collected from the column output during the breakthrough curve for further analysis in a silica-gel chromatographic column.

Prior to each run, the packed bed is regenerated for at least 2 hr at 423 K under helium flow up to 50 ml/min. The next experiment can start as soon as the TCD signal is stable again. In our experimental procedure first experiments were not taking into account. The reversibility is evaluated by repeating some experiments occasionally and verifying the amount adsorbed which generally agree well. In this work, two columns with different internal diameters were used for single and multicomponent experiments. The characteristics of these adsorption units are reported in Table 2.

Table 2. Fixed-bed parameters and adsorbent properties used in the modelling of the sorption experiments of N_2, CH_4 and CO_2 in MOF-508b

Fixed bed parameters	Single experiments	Multicomponent experiments
Bed diameter, d [m]	0.0046	0.0077
Bed length, L [m]	0.10	0.10
Bed porosity, ε_b [−]	0.74	0.68
Bulk density, ρ_b [kg/m^3]	390.5	470.7
Mass of adsorbent, W[g]	0.649	2.192
Particle diameter, d_p [μm]	25–100	
Particle density, ρ_a [kg/m^3]	1492	

MODELING ADSORPTION EQUILIBRIUM

Pure Component Isotherms

From the engineering point of view, it is important to have a good analytical description of the equilibrium data in order to reduce experimentation. The simplest theoretical model for monolayer adsorption was proposed by Langmuir (5) and it can be represented by the following equation:

$$q(p,T) = q_m \cdot \frac{b(T) \cdot p}{1 + b(T) \cdot p} \tag{1}$$

where q is the amount adsorbed, p is the partial pressure of the adsorbate, b and q_m are the adsorption affinity constant and the saturation loading, respectively. This model is based on the assumptions that the surface of the adsorbent is energetically homogeneous and the adsorbate occupies one active site when it adsorbs which is reasonable when the adsorbate molecule is small. Adsorption affinity constant, b, is assumed to vary with temperature according to the following equation:

$$b = b_0 \cdot e^{\left(\frac{-\Delta H}{RT}\right)} \tag{2}$$

where b_0 is the frequency factor of the affinity constant, ΔH is the heat of sorption, R is the universal gas constant and T is the temperature.

The parameters of the Langmuir isotherm for the three gases on MOF-508b are determined by numerical procedure. The mean absolute deviations, $\bar{\Delta}q$, between the predicted, q, and the experimental, q_{exp},

values are calculated with:

$$\bar{\Delta}q = \frac{1}{N}\sum_{i=1}^{N}\sqrt{(q_{\exp,i} - q_i)^2} \tag{3}$$

being N the total number of measurements.

Multicomponent Adsorption Isotherms

Using the parameters given by the single component adsorption equilibrium fitting, the mixture sorption data can be predicted by an extended Langmuir isotherm model. Accordingly, the amount adsorbed of component i, q_i, in a mixture is given by:

$$q_i(p,T) = q_{m,i} \cdot \frac{b_i\ (T) \cdot p_i}{1 + \sum_{k=1}^{n} b_k\ (T) \cdot p_k} \tag{4}$$

where n is the number of components present in the mixture.

Modeling

The adsorption system is a column packed with crystals of MOF-508b through which an inert gas flows in steady-state. At time zero an adsorbate flow of known composition and an inert are introduced at the bottom of column. Several simplifications were introduced to reduce the computational time, thus the following assumptions are made:

1. The gas phase behaves as an ideal gas mixture;
2. The pressure drop through the bed is negligible;
3. The flow pattern is described by the axially dispersed plug flow model;
4. The main resistances to mass transfer for adsorbable species can be combined in a lumped mass transfer coefficient;
5. The column is isothermal.

According to these assumptions, the equations used to simulate single and multicomponent breakthrough curves are summarized in Table 3.

The Linear Driving Force (LDF) model used in this work has been tested successfully in previous studies (6,7) to simulate breakthrough curves of alkanes in zeolitic materials. The set of equations was solved numerically using the orthogonal collocation method (8). The resulting system was solved using a fifth-order Runge-Kutta code in conjunction with a Gauss elimination (algebraic equations). Twelve collocation points

Table 3. Dynamic mathematical model equations for fixed bed adsorption

	Equations	
Mass balance to sorbate species	$\varepsilon_b D_L \frac{\partial}{\partial z}\left(C\frac{\partial y_a}{\partial z}\right) = \frac{\partial (F y_a)}{\partial z} + \varepsilon_b \frac{\partial (C y_a)}{\partial t} + (1-\varepsilon_b)\rho_a \frac{\partial \bar{q}_i}{\partial t}$	(5)
Boundary conditions:	$z = 0, t > 0 \quad \varepsilon_b D_L C \frac{\partial y_a}{\partial z} = F y_a - F_f y_{af}$	(5a)
	$z = L, t > 0 \quad \frac{\partial y_a}{\partial z} = 0$	(5b)
Overall mass balance	$\frac{\partial F}{\partial z} + \varepsilon_b \frac{\partial C}{\partial t} + \sum_{i=1}^{N}(1-\varepsilon_b)\rho_a \frac{\partial \bar{q}_i}{\partial t} = 0$	(6)
Boundary condition	$z = 0, t > 0 \quad F = F_f$	(6a)
Mass transfer rate	$\frac{\partial \bar{q}_i}{\partial t} = k(q_i - \bar{q}_i)$	(7)
Axial dispersion (Wakao and Funazkri, 1978) (9)	$D_L = \frac{20}{\varepsilon_b} D_m + \frac{u d_c}{2}$	(8)

gave a good accuracy for all experiments. The parameters used to predict the experimental data are summarized in Table 1.

Estimation of Model Parameters for Experimental Breakthrough Curves

In order to fit the experimental breakthrough curves, numerical values for both axial dispersion and lumped mass transfer coefficients are required. The axial dispersion coefficients for each of the runs were estimated from the correlation given by Wakao and Funazkri (9) (see Table 3). This correlation follows from experiments in the low Reynolds number regime ($Re < 2$) with sufficiently rapid adsorption within the particle. In the present study, small crystals ($25\,\mu m < d_p < 100\,\mu m$) in a non-pelletized form were used resulting in a fast kinetic, moreover, the Reynolds number from the different runs was in the range $0.1 < Re < 0.6$. Therefore, the Wakao correlation was used to predict the axial dispersion. This correlation has been already used in the modeling of pressure swing adsorption separation of mixtures CH_4, CO_2 and N_2 (10).

The lumped mass transfer coefficients for the experimental runs were estimated from the following correlation (11):

$$k = \left(\frac{d_p q_0}{6 k_f c_0} + \frac{d_p^2}{60 D_c}\right)^{-1} \tag{9}$$

which consider micropore and film resistances to mass transfer. The macropore diffusion mechanisms were neglected since we are dealing

with non-binded microporous crystals dispersed on an inert glass wool. The contribution of the external film for the mass transport resistance was taken into account despite the fact that its importance is two orders of magnitude lower than the micropore mass transport resistance. An average crystal radius of 31 μm was considered. The values for the ratio q_0/c_0 were obtained from the equilibrium model. The external mass transfer coefficient, k_f, was given by (12):

$$k_f = \frac{u}{Sc^{2/3}}\left(\frac{0.765}{(\mathrm{Re}\ \varepsilon_b)^{0.82}} + \frac{0.365}{(\mathrm{Re}\ \varepsilon_b)^{0.386}}\right) \tag{10}$$

where u is the interstitial velocity, Re the particle Reynolds number, both calculated with the feed flow rate and Sc is the Schmidt number. Molecular diffusivity was estimated from the Chapman-Enskog equation.

The micropore diffusivity, D_c in Equation (9) was used as a temperature dependent fitting parameter for the simulated pure component breakthrough curves, since is the only unknown term of the mathematical model. The value of D_c follows the expression:

$$D_c = D_0 \exp(-E_a/RT) \tag{11}$$

where, D_0 is the pre-exponential factor and E_a is the diffusional activation energy. The micropore diffusivity fitted for single component breakthrough curves was also used to predict the binary and ternary experiments.

RESULTS AND DISCUSSION

Pure Component Isotherms

The first step in the characterization of an adsorbent for a specific separation process is the measurement of the adsorption equilibrium of pure components. Pure component isotherms were determined from breakthrough experiments performed with single components diluted in helium used as the inert carrier gas. The loading was determined by numerical integration of the breakthrough data following the procedure describe in previous works (6). The experiments were performed at temperatures of 303 K, 323 K, and 343 K and partial pressures between 0.1 and 4.5 bar. Complete information of the experimental fixed-bed runs performed, including partial pressure, temperature, flowrate, mass of adsorbent used in the column, and the amount adsorbed for each run by the integration of the molar flowrate histories, is shown in Table 4.

Table 4. Experimental conditions and dynamic model parameters for single component breakthrough curves of N_2, CO_2 and CH_4

Run	T (K)	p (bar)	P (bar)	V_{Helium} (ml/min)	q (mmol/g_{ads})	k (s^{-1})	D_L (10^{-4} m^2/s)	D_c (10^{-11} m^2/s)	E_a (kJ/mol)
N_2									
1	303	0.10	2	43.1	0.08	0.46	7.4	3.0	6.2
2		0.53	5	30.3	0.41	0.46	3.0		
3		1.00	5	26.9	0.65	0.46	3.0		
4		2.01	5	19.2	1.00	0.46	3.0		
5		3.04	5	13.2	1.42	0.46	3.0		
6		4.52	5	3.0	1.95	0.46	3.0		
7	323	0.10	2	48.2	0.08	0.54	8.2	3.5	
8		0.50	5	35.7	0.37	0.54	3.3		
9		0.94	5	26.2	0.60	0.54	3.3		
10		2.01	5	19.5	0.97	0.54	3.3		
11		3.03	5	13.7	1.39	0.54	3.3		
12		4.61	5	2.8	1.96	0.54	3.3		
13	343	0.13	2	49. 4	0.09	0.61	9.1	4.0	
14		0.56	5	34.9	0.37	0.61	3.6		
15		1.02	5	27.7	0.57	0.61	3.6		
18		2.05	5	21.8	0.95	0.61	3.6		
17		3.03	5	13.7	1.35	0.61	3.6		
18		4.51	5	3.2	1.90	0.61	3.6		
CH_4									
19	303	0.15	2	40.2	0.17	0.46	7.4	3.0	6.2

20		0.55	5	29.7	0.42	0.46	3.0		
21		1.03	5	26.4	0.64	0.46	3.0		
22		2.04	5	19.6	1.05	0.46	3.0		
23		3.04	5	13.4	1.47	0.46	3.0		
24		4.51	5	3.3	1.98	0.46	3.0		
25	323	0.13	2	38.9	0.15	0.54	8.2	3.5	
26		0.54	5	29.2	0.38	0.54	3.3		
27		1.03	5	25.9	0.60	0.54	3.3		
28		2.06	5	19.6	0.99	0.54	3.3		
29		3.05	5	13.0	1.38	0.54	3.3		
30		4.52	5	2.9	1.87	0.54	3.3		
31	343	0.12	2	38.5	0.13	0.61	9.1	4.0	
32		0.53	5	31.4	0.36	0.61	3.7		
33		1.05	5	26.4	0.59	0.61	3.7		
34		2.05	5	19.7	0.95	0.61	3.7		
35		2.96	5	12.9	1.31	0.61	3.7		
36		4.52	5	3.0	1.84	0.61	3.7		
CO_2									
37	303	0.11	2	45.4	0.20	7.58	6.1	50	3.9
38		0.46	5	31.9	0.96	7.47	2.5		

(*Continued*)

Table 4. Continued

Run	T (K)	p (bar)	P (bar)	V_{Helium} (ml/min)	q (mmol/g_{ads})	k (s^{-1})	D_L (10^{-4} m^2/s)	D_c (10^{-11} m^2/s)	E_a (kJ/mol)
39		1.00	5	25.6	1.78	7.47	2.5		
40		2.04	5	19.1	3.07	7.48	2.5		
41		3.04	5	13.8	4.25	7.50	2.5		
42		4.52	5	3.1	5.93	7.51	2.5		
43	323	0.10	2	47.5	0.14	8.37	6.7	55	
44		0.47	5	33.5	0.67	8.29	2.7		
45		1.04	5	25.6	1.28	8.29	2.7		
46		2.03	5	20.3	2.13	8.30	2.7		
47		3.06	5	13.4	2.96	8.30	2.7		
48		4.51	5	3.0	3.95	8.31	2.7		
49	343	0.11	2	47.8	0.11	9.16	7.5	60	
50		0.52	5	32.5	0.54	9.09	3.0		
51		1.01	5	27.1	0.90	9.09	3.0		
52		2.04	5	21.9	1.55	9.10	3.0		
53		3.04	5	13.8	2.12	9.10	3.0		
54		4.52	5	3.3	2.96	9.10	3.0		

Figure 3 shows the adsorption equilibrium isotherms plotted in terms of the loading in mmol/gads as a function of the partial pressure. It can be seen from the figure that the isotherms are Type I in IUPAC classification. The saturation was not reached because of operating pressure limitations in our setup. The equilibrium data shows that CO_2 is much more adsorbed than CH_4 and N_2. This difference is considerably higher at 303 K but it decrease significantly when the temperature is increased. The one-dimensional 4.0×4.0 Å channels in MOF-508b seems large

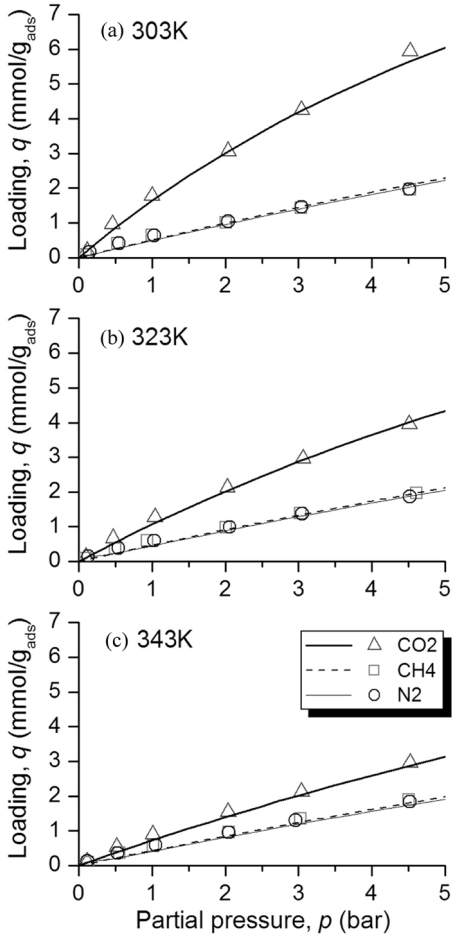

Figure 3. Pure component adsorption equilibrium isotherm of CO_2, CH_4 and N_2 at (a) 303 K, (b) 323 K and (c) 343 K on 4 MOF-508b. The continuous lines represent the fitting with the Langmuir model. *Isotherm model parameters in Table 5*.

enough to neglect shape selectivity effects when compared with the kinetics diameters of the gas molecules. Moreover, the van der Waals interaction surfaces of the three gases are too much close to being the reason for such difference. However, the large quadrupolar moment and polarizability of CO_2 are predominantly the cause of the difference in adsorption behavior (Table 1). The quadrupole moment produces a strong attraction to the adsorbent surface resulting in a higher uptake (13). The high level of polarizability of CO_2 and CH_4 can create a momentary shift in its neutral electrostatic field when the molecule is close to the metallic sites of the structure. Nevertheless, this attraction force is much weaker than the quadrupole moment. The nitrogen molecule also exhibits a quadrupolar moment but its magnitude is much lower than the one for CO_2.

Another interesting feature that can be seen in Fig. 3 is the absence of steps in all the adsorption isotherms and for the entire range of partial pressure and temperature studied in this work. Such effect is often due to structural transformations which can include for example "breathing" and scissoring mechanisms (14–16). These transformations can make impracticable the utilization of MOFs in industrial processes because the pellets can crumble if the framework undergoes a cell volume change. A consequence of such phenomena could be a sharp increasing of the pressure drop in the column, which can result in serious damages in the equipment.

The fitted pure component isotherms with the Langmuir model are the lines in Fig. 3. Langmuir parameters obtained from numerical optimization, as well as the mean absolute deviations between experimental data and predicted values are shown in Table 5. The saturation loading for the three components were kept constant during the optimization procedure; such restriction allows giving thermodynamic consistency to the isotherm model (17). The fitted value for the saturation capacity, $q = 18.34\,\text{mmol/g}$, is similar to the ones found in MOF materials with larger pores (18). The heat of adsorption fitted by numerical procedure for CO_2 (18.8 kJ/mol) is 5 times higher than the ones for CH_4 and N_2 ($\sim$3.7 kJ/mol). However, these values are lower than those found in porous MOFs (15). This enthalpy difference can be related to endothermic processes which involve structural transformations caused by the flexibility of MOF-508b. Such endothermic framework transformation, to some extent, compensates the exothermic adsorption behaviour as rationalized in MIL-53 (15), leading to the low heats of sorption in MOF-508b. It is clear from Fig. 3 that the Langmuir model is reasonable in predicting isotherm sorption behavior of pure CO_2, CH_4, and N_2 in the range of temperatures and partial pressures studied.

Binary Adsorption Isotherms

Figures 4(a–c) and 4(d–f) show the binary adsorption isotherms for an equimolar mixtures of CO_2/N_2 and CO_2/CH_4, respectively. The experiments were performed at 303 K, 323 K, and 343 K and partial pressure up to 2 bar. The experimental conditions for binary experiments as well as the amount adsorbed are given in Table 6.

In both equimolar mixtures, Fig. 4 shows a large difference relatively to the loading of CO_2 which significantly decreases as the temperature increases. Also, at the same time that the loading of CO_2 decreases, the amounts adsorbed of CH_4 and N_2 remain practically unchanged

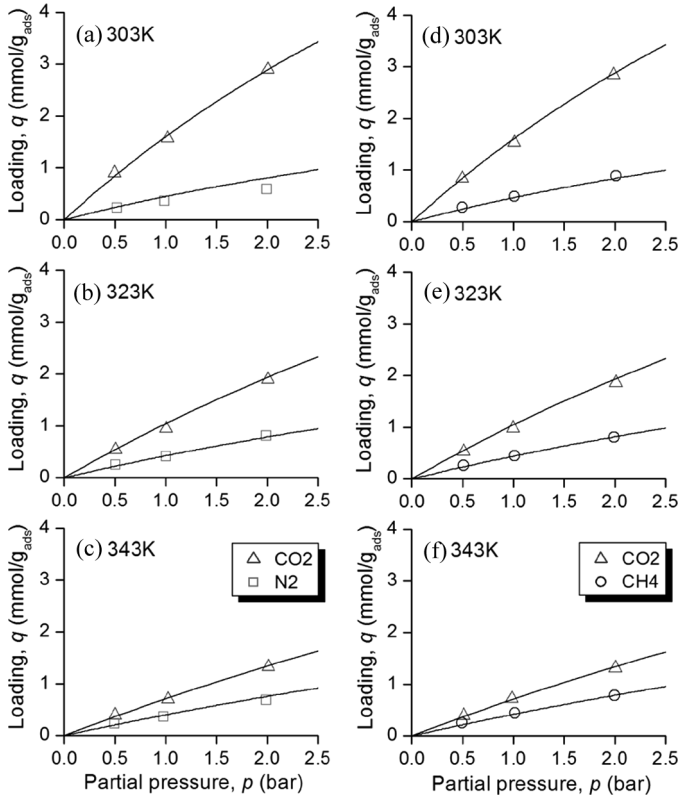

Figure 4. Binary adsorption equilibrium isotherms for equimolar mixtures of (a–c) N_2–CO_2 and (d–f) CH_4–CO_2 on 4 MOF-508b at 303 K, 323 K and 343 K. The continuous lines represent the prediction of the Langmuir model. *Isotherm model parameters in Table 5.*

Table 5. Langmuir model parameters and deviations between model and experiments

Parameter	Unit	N_2	CH_4	CO_2
q_m	(mmol/g_{ads})	18.34	18.34	18.34
b_0	(bar^{-1})	6.37×10^{-3}	6.73×10^{-3}	5.64×10^{-5}
b (303 K)	(bar^{-1})	0.027	0.029	0.098
b (323 K)	(bar^{-1})	0.025	0.026	0.062
b (343 K)	(bar^{-1})	0.023	0.024	0.041
$-\Delta H$	(kJ/mol)	3.70	3.65	18.80
$\overline{\Delta q}$	(mmol/g_{ads})	0.098	0.084	0.098

strengthening the idea that quadrupole moment of CO_2 plays an important role in this separation.

We also note that the extended Langmuir model prediction represented by the lines in Fig. 4 gives a proper description of the binary adsorption data.

Ternary Adsorption Isotherms

Figure 5(a–c) shows the ternary adsorption isotherms for an equimolar mixture $CO_2/CH_4/N_2$. The experiments were performed at 303 K, 323 K, and 343 K and partial pressure up to 1.4 bar.

As shown in Fig. 5, the adsorption behavior does not seem to be affected by the simultaneous presence of the tree gases in the adsorbent structure when compared with the binary experiments. The adsorption capacities of MOF-508b decrease in the following order $CO_2 \gg CH_4 > N_2$. The CO_2 uptake is significantly dependent on the temperature decreasing as the temperature increases. Conversely, adsorption capacities for CH_4 and N_2 in MOF-508b are almost independent of the temperature. Such difference in temperature dependence of the adsorption behaviors might be specifically useful to optimize the operating conditions for the CO_2 removal from natural gas.

Once more, the experimental sorption isotherms are predicted by the Langmuir model.

Modeling of the Single Breakthrough Experiments

The comparison between experimental and theoretical pure component breakthrough curves is shown in Fig. 6 for CO_2, CH_4, and N_2 in terms of the adsorbate mol fraction in the gas phase at the outlet of the column

Table 6. Experimental conditions and dynamic model parameters for breakthrough curves of binary mixtures CH_4/CO_2 and N_2/CO_2 and ternary mixtures $N_2/CH_4/CO_2$; mean absolute deviations between predicted (extended Langmuir) and measured adsorption equilibria on MOF-508b

				V (ml/min)				q (mmol/g_{ads})			k (s^{-1})			
Run	T (K)	P (bar)	V_{Helium} (ml/min)	N_2	CH_4	CO_2	p_{mix} (bar)	N_2	CH_4	CO_2	N_2	CH_4	CO_2	D_L (10^{-4} m^2/s)
b1_1	303	5	27.8	–	3.4	3.4	1	–	0.28	0.84	–	0.46	7.45	2.8
b1_2		5	19.5	–	6.6	6.6	2	–	0.49	1.53	–	0.46	7.45	2.7
b1_3		5	6.0	–	11.9	11.8	4	–	0.89	2.84	–	0.46	7.45	2.5
b1_4	323	5	28.5	–	3.6	3.6		–	0.26	0.53	–	0.54	8.28	3.1
b1_5		5	20.0	–	6.8	6.7	2	–	0.45	0.98	–	0.54	8.27	2.9
b1_6		5	6.2	–	12.4	12.5	4	–	0.81	1.86	–	0.54	8.26	2.7
b1_7	343	5	28.7	–	3.5	3.7	1	–	0.25	0.39	–	0.61	9.08	3.4
b1_8		5	19.7	–	6.7	6.5	2	–	0.44	0.72	–	0.61	9.08	3.2
b1_9		5	6.2	–	12.4	12.5	4	–	0.78	1.31	–	0.61	9.07	3.0
b2_1	303	5	28.6	3.7	–	3.6	1	0.23	–	0.90	0.46	–	7.45	2.6
b2_2		5	19.9	6.6	–	6.8	2	0.36	–	1.57	0.46	–	7.44	2.4
b2_3		5	6.5	13	–	13	4	0.59	–	2.89	0.46	–	7.44	2.1
b2_4	323	5	28.7	3.7	–	3.6	1	0.25	–	0.54	0.54	–	8.27	2.9
b2_5		5	19.4	6.5	–	6.5	2	0.41	–	0.95	0.54	–	8.26	2.7
b2_6		5	6.4	12.8	–	12.8	4	0.81	–	1.89	0.54	–	8.25	2.3
b2_7	343	5	28.7	3.6	–	3.6	1	0.23	–	0.39	0.61	–	9.08	3.2
b2_8		5	19.0	6.2	–	6.5	2	0.36	–	0.70	0.61	–	9.07	3.0
b2_9		5	6.5	13.0	–	13.2	4	0.68	–	1.32	0.61	–	9.05	2.6

(*Continued*)

Table 6. Continued

Run	T (K)	P (bar)	V_{Helium} (ml/min)	V (ml/min)			p_{mix} (bar)	q (mmol/g_{ads})			k (s^{-1})			D_L (10^{-4} m^2/s)
				N_2	CH_4	CO_2		N_2	CH_4	CO_2	N_2	CH_4	CO_2	
t_1	303	5	19.6	4.3	4.3	4.3	2	0.25	0.31	1.05	0.46	0.46	7.42	2.2
t_2		5	12.6	6.3	6.4	6.4	3	0.31	0.42	1.50	0.46	0.46	7.40	2.0
t_3		5	6.4	8.5	8.6	8.6	4	0.36	0.49	2.01	0.46	0.46	7.39	1.8
t_4	323	5	19.8	4.5	4.4	4.4	2	0.26	0.29	0.62	0.54	0.54	8.25	2.5
t_5		5	12.5	6.3	6.2	6.1	3	0.36	0.41	0.88	0.54	0.54	8.23	2.2
t_6		5	6.2	8.3	8.3	8.4	4	0.49	0.55	1.21	0.54	0.54	8.22	2.0
t_7	343	5	19.3	4.3	4.3	4.3	2	0.26	0.28	0.43	0.61	0.61	9.06	2.7
t_8		5	12.6	6.3	6.3	6.3	3	0.33	0.36	0.61	0.61	0.61	9.05	2.4
t_9		5	6.3	8.4	8.3	8.4	4	0.44	0.48	0.80	0.61	0.61	9.03	2.2
				Binary mixtures							*Ternary mixture*			
				$CO_2 + N_2$			$CO_2 + CH_4$				$CO_2 + CH_4 + N_2$			
$\overline{\Delta q}$ (mmol/g_{ads})				*0.049*			*0.028*				*0.059*			

b, Binary experiment; *t*, Ternary experiment.

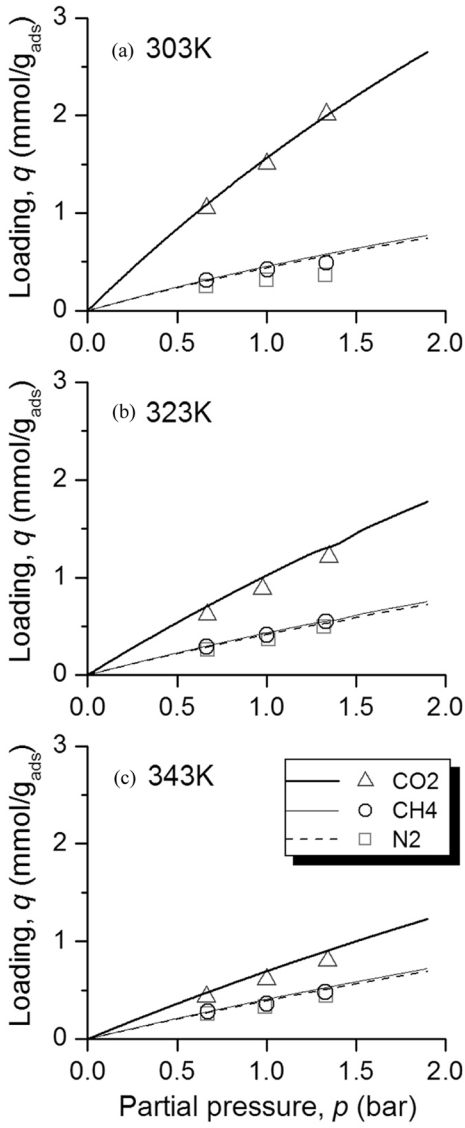

Figure 5. Ternary adsorption equilibrium isotherms for an equimolar mixture of $CO_2/CH_4/N_2$ on 4 MOF-508b at a) 303 K, b) 323 K and c) 343 K. The lines represent the prediction of the Langmuir model. *Isotherm model parameters in Table 5*.

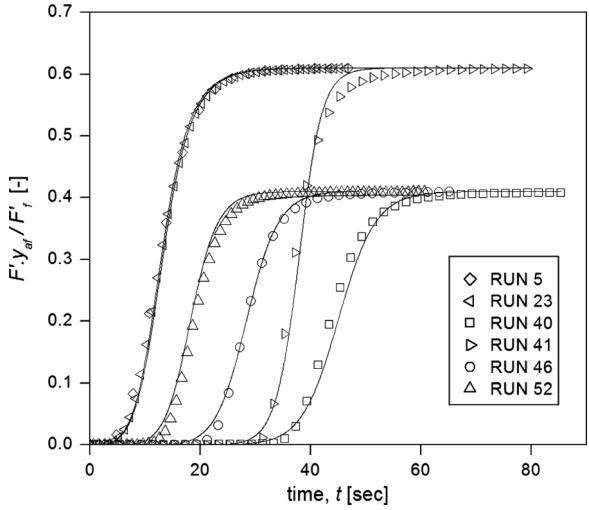

Figure 6. Pure component breakthrough curves of CO_2, CH_4 and N_2 in 4 MOF-508b. Experimental conditions are in Table 4. Continuous lines are obtained with the mathematical model. N_2, run 5; CH_4, run 23; CO_2, runs 40, 41, 46 and 52.

as a function of the time. The experimental conditions are detailed in Table 4. The sharpness of the breakthrough curves indicates a fast kinetics which is good for the development of separation processes based on equilibrium properties.

The experimental breakthrough curve was matched by fitting the micropore diffusion parameter, D_c. The estimated diffusional parameters, listed in Table 4, were considered to be independent of the loading since the experimental conditions still far from the saturation region. The micropore diffusion within the channels of MOF-508b for CO_2 (D_c $(303\,K) = 5 \times 10^{-10}\,m^2/s$) is one order of magnitude faster than for CH_4 and N_2. Such results can be explained by the fact that the kinetic diameter of CH_4 and N_2 is greater than the one of CO_2 (see Table 1). In a general way, the diffusivity of the molecules studied in this work is lower than the ones reported in the literature for MFI (19,20); for instance, Krishna and Baten (20) have determined by molecular dynamic simulation diffusivity values ranging from 10^{-9} to $10^{-8}\,m^2/s$ for CO_2, CH_4 and N_2 in MFI at $T = 300\,K$. This difference can also be explained by the relation between the molecular diameter and the pore dimension since the channels of MFI ($5.1 \times 5.6\,Å$) are larger than the ones of MOF-508b ($4.0 \times 4.0\,Å$), consequently the diffusion can be faster in the first case. The temperature dependence of the intra-crystalline diffusion

in MOF-508b was found to be very low for the three molecules as it can be seen from the diffusional activation energy, E_a, listed in Table 4. Data reported in the literature for micropore diffusion of CO_2, CH_4 and N_2 in zeolite 4 A at 303 K show values in the order $10^{-12}\,m^2/s$ with activation energies for diffusion around 20 kJ/mol for the three molecules (23). Taking into account the similarity of the pore dimension of both adsorbents, and the high diffusivity found in MOF-508b, the diffusion mechanism in this metal-organic framework can be characterized as "fast diffusion" and this can explain the low activation energy found.

From the practical point of view, this approach for the estimation of the diffusional parameters seems fair considering the explanation given in a previous section; nevertheless, results should be read with caution since they were obtained form the match of breakthrough curves.

Figure 6 shows clearly that the dynamic mathematical model reproduces very well the experimental data for the temperature and feed concentration range studied in this work.

Modeling of the Binary Breakthrough Experiments for Equimolar Mixtures CO_2/CH_4 and CO_2/N_2

In practice we wish to separate the CO_2 molecules from CH_4 and N_2 in a fixed bed. In this section we give an overview of the typical multicomponent breakthrough curves obtained. In Fig. 7, the breakthrough curves of a binary equimolar mixture of CO_2/CH_4 are shown for the temperatures 303 K, 323 K, and 343 K and total adsorbate pressure around 2 bar. We plot the breakthrough curves in terms of the normalized mass flow of the adsorptive species F'/F'_f, as a function of time. Interesting to note that for $T = 303$ K, methane appears at the outlet of the column at a time of approximately 40 sec compared to a time value of 100 sec for CO_2. This time difference is suitable for a separation in a fixed bed. For the mixture CO_2/N_2 the separation degree is quite similar as can be seen in Fig. 8. This result allows us to conclude that the separation degree observed between these isomers can lead to the development of a separation process by adsorption.

Figures 7 and 8 also shows some dispersion in the shape of breakthrough curves and this is due to a combined effect of mass transfer resistance, and axial dispersion. The dynamic model parameters of the LDF-based mathematical model can be seen in Table 6. The value k can be considered as lumped parameters. It can be concluded from the multicomponent breakthrough experiments that this simple model does a good job for the prediction of both dispersion and overshoot phenomena.

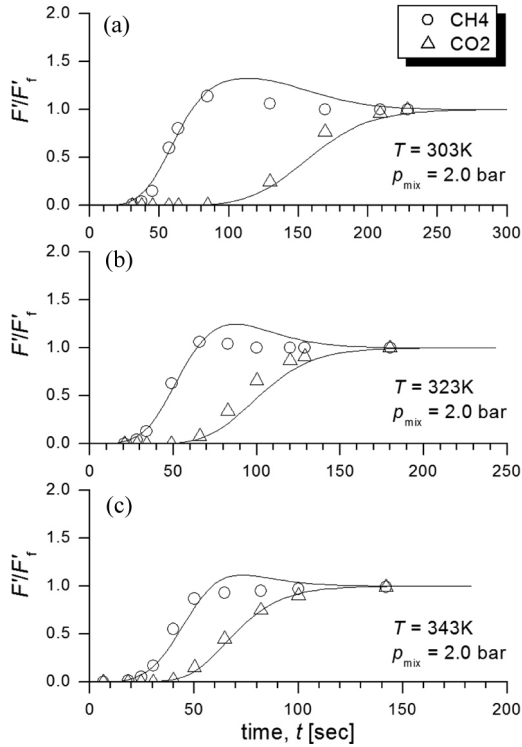

Figure 7. Effect of temperature on binary breakthrough curves for equimolar mixtures of CH_4–CO_2 at *a*) T = 303 K, *b*) T = 323 K and *c*) T = 343 K at a total mixture pressure around 2 bar. Total system pressure was fixed at 5 bar. *Experimental conditions and model parameters in Table 6. Lines represent the dynamic mathematical model simulation and points are experimental data.*

Modeling of the Ternary Breakthrough Experiments for Equimolar Mixtures $CO_2/CH_4/N_2$

The breakthrough curves in Fig. 9 show that N_2 leaves the bed slightly before CH_4. The last component to go out, CO_2, is clearly the most strongly adsorbed component which explains the difference in the amount adsorbed of CO_2 relatively to the other components, already observed in the ternary adsorption equilibrium isotherms shown in Fig. 5.

The agreement between experimental data and the mathematical model is reasonably good, and this is remarkably taken into consideration that we are using a simple LDF model in a simulation of a

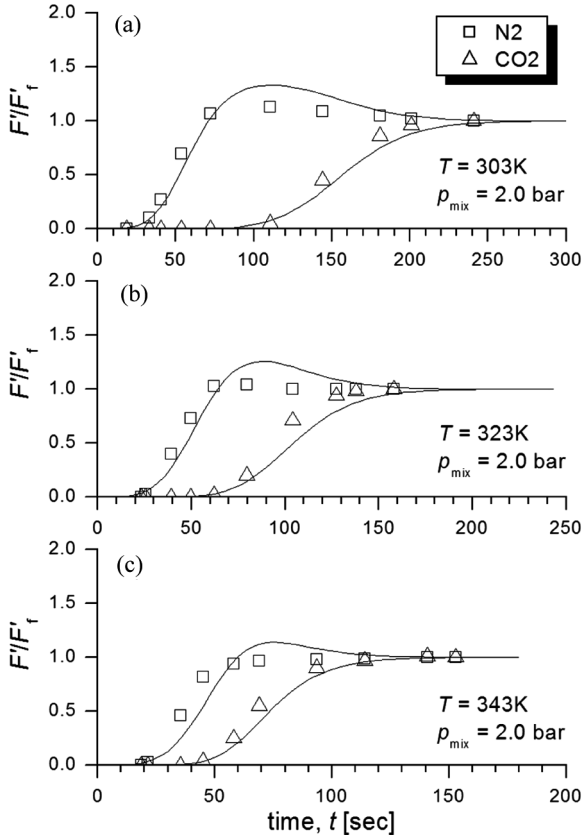

Figure 8. Effect of temperature on binary breakthrough curves for equimolar mixtures of N_2–CO_2 at *a*) T = 303 K, *b*) T = 323 K and *c*) T = 343 K at a total mixture pressure around 2 bar. Total system pressure was fixed at 5 bar. *Experimental conditions and model parameters in Table 6. Lines represent the dynamic mathematical model simulation and points are experimental data.*

nonlinear multicomponent system of three adsorbable species in a complex metal-organic structure.

The separation potential of an equimolar mixture can be described in terms of the sorption selectivity, S, defined on a molar basis by $S = q_1/q_2$, where compound 1 is more adsorbed. Figure 10 shows the effect of temperature and mixture pressure on the sorption selectivity a) $S_{CO2/CH4}$ and b) $S_{CO2/N2}$ for a ternary equimolar mixture $CO_2/CH_4/N_2$ on MOF-508b. In both cases, the drop in temperature favor the selectivity. For the three temperatures, we can see that the selectivity is higher for the mixture

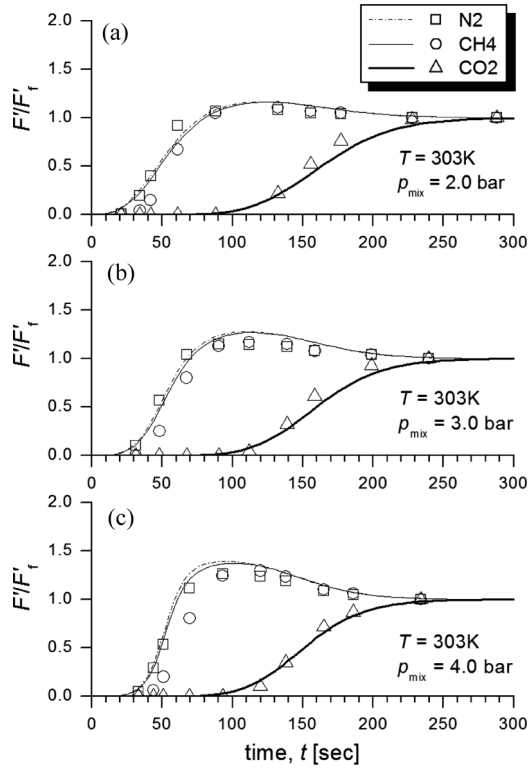

Figure 9. Effect of partial pressure on ternary breakthrough curves for equimolar mixtures of $N_2-CH_4-CO_2$ at $T = 303\,K$ and *a*) $p_{mix} = 2.0\,bar$, *b*) $p_{mix} = 3.0\,bar$ and *c*) $p_{mix} = 4.0\,bar$. Total system pressure was fixed at 5 bar. *Experimental conditions and model parameters in Table 6. Lines represent the dynamic mathematical model simulation and points are experimental data.*

CO_2/N_2; also the mixture pressure does not seems to have significant influence on the sorption selectivity, except at 303 K where a slight increase is observed.

Note that the predictions of the extended Langmuir model (lines in Fig. 10) give pressure-independent values for the selectivities $S_{CO2/CH4}$ and $S_{CO2/N2}$, indicating the absence of competition for the active sites between the three types of gas molecules studied. However, the slight increase previously mentioned for the experimental data at 303 K requires some experiments at mixture pressure higher than 4 bar in order to check if the cause of this phenomenon is or not related to an experimental problem.

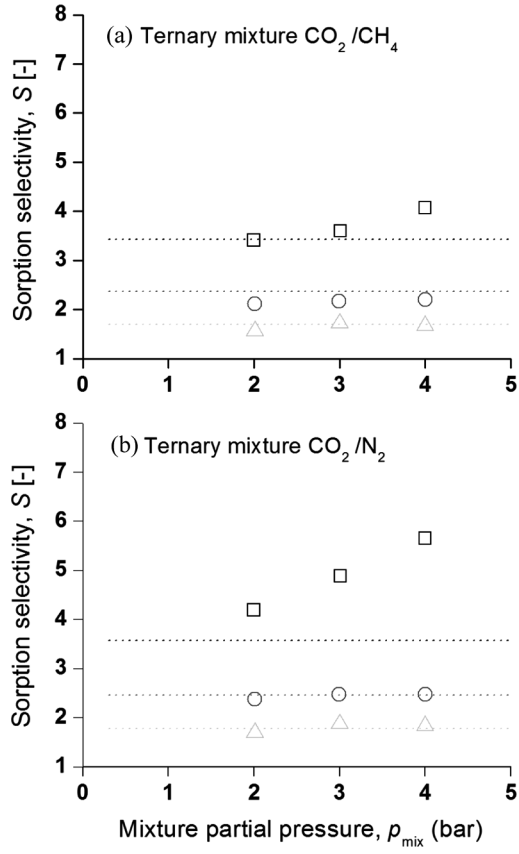

Figure 10. Temperature-dependent sorption selectivity for (a) CO_2/CH_4 and (b) CO_2/N_2 in equimolar ternary $CO_2/CH_4/N_2$ mixtures, as function of the mixture partial pressure (□, T = 303 K; ○, T = 323 K; Δ, T = 343 K). *Points are experimental data and lines represent the sorption selectivity predicted by the Langmuir model.*

CONCLUSIONS

The adsorption and separation of CO_2, CH_4, and N_2 on MOF-508b by fixed bed process have been studied. Single and multicomponent equilibrium data have been obtained through experimental breakthrough curves in a temperature range comprised between 303 K and 343 K. The gas partial pressure has been increased up to 4.5 bar without reaching the saturation stage.

The single isotherm data was fitted with good accuracy by a simple Langmuir model. The Langmuir model parameters were used to predict the multicomponent equilibrium giving a well description of the adsorption behavior of the gas mixture on MOF-508b. A model based on the LDF approximation which has taken into account the isotherm model predictions was able to described both mono- and multicomponent experimental breakthrough curves. The micropore diffusivity estimated by the dynamic mathematical model gives values of the order of $10^{-10}\,m^2/s$ for CO_2 and $10^{-11}\,m^2/s$ for CH_4 and N_2.

The experiments performed allow concluding that MOF-508b is a highly selective material for CO_2 separation at room temperature. If the rise in temperature causes a sharp decrease in CO_2 affinity, on the other hand the change in partial pressure seems to not have a strong influence. The low amount adsorbed of CH_4 and N_2 are practically temperature independent offering a large range of operating conditions favorable to the CO_2 removal from natural gas. The sharpness in breakthrough curves indicates a fast kinetic which contribute to the short regeneration time of MOF-508b.

These results show that MOF-508b can be a suitable adsorbent for the development of processes for CO_2 separation from natural gas.

ACKNOWLEDGEMENTS

This work was supported by an Award CHE 0718281 from the National Science Foundation (B.C.), the University of Texas-Pan American (UTPA) through a Faculty Research Council Award (B.C), in part by the Welch Foundation (Grant BG-0017) to the Department of Chemistry at UTPA. J.A.C.S. acknowledges financial support provided by national research grant FCT/POCTI/EQU/60828/2004 and by LSRE financing by FEDER/POCI/2010. P.S.B. acknowledges his Ph.D. scholarship by FCT (SFRH/BD/30994/2006), and L.B. acknowledges Henri Pieper Grant (Institute HEMES Gramme, Belgium) for the financial support.

NOTATION

b	affinity constant (bar^{-1})
b_0	frequency factor of the affinity constant (bar^{-1})
c_0	molar gas concentration at the inlet of the fixed bed (mol/m^3)
c_i	molar concentration of sorbate species i in the bulk gas phase (mol/m^3)
C	total molar gas concentration in bulk gas phase (mol/m^3)

d	column diameter (m)
d_p	particle diameter (m)
D_c	micropore diffusivity (m^2/s)
D_L	axial dispersion coefficient in fixed bed (m^2/s)
D_m	molecular diffusivity (m^2/s)
D_0	pre-exponential factor (m^2/s)
E_a	diffusional activation energy (kJ/mol)
F'	molar rate of adsorptive species at the column outlet (mol/s)
F_f'	molar rate of the adsorptive species in the feed (mol/s)
F	total molar flux (mol/(m^2.s))
F_f	total molar flux of feed (mol/(m^2.s))
ΔH	adsorption enthalpy (J/mol)
k	mass transfer coefficient (s^{-1})
k_f	external film mass transfer coefficient (m/s)
L	column length (m)
p	partial pressure (bar)
P	total system pressure (bar)
q	adsorbed concentration of sorbate in the adsorbent particle (mmol/g)
$\bar{q}$	average adsorbed concentration of sorbate in adsorbent particle (mmol/g)
q_m	saturation loading capacity of sorbate in the adsorbent (mmol/g)
R	gas constant (kJ/mol/K)
Re	Reynolds number (−)
Sc	Schmidt number (−)
t	time (s)
T	temperature (K)
u	interstitial velocity in packed bed (m/s)
W	mass of adsorbent in the column (kg)
y_a	mole fraction of the sorbate in the bulk phase (−)
y_{af}	mole fraction of the sorbate at the inlet of the column (−)
z	distance coordinate along fixed bed (m)

Greek Letters

ρ_a	apparent density (kg/m^3)
ρ_b	bulk density (kg/m^3)
ε_b	bulk porosity (−)

REFERENCES

1. Hugman, R.H.; Vidas, E.H.; Springer, P.S. (1993) *Chemical Composition of Discovered and Undiscovered Natural Gas in the United States*; Gas Research Institute: Chicago, Illinois.

2. Lokhandwala, K.A.; Baker, R.W.; Toy L.G.; Amo K.D. Sour Gas Treatment Process Including Dehydration of the Gas Stream. U.S. Patent 5,401,300, March 28, 1995.
3. Bastin, L.; Bárcia, P.S.; Hurtado, E.J.; Silva, J.A.C.; Rodrigues, A.E.; Chen, B. (2008) A microporous metal-organic framework for separation of CO2/N2 and CO2/CH4 by fixed-bed. *J. Phys. Chem. C.*, *112* (5): 1575.
4. Chen, B.; Liang, C.; Yang, J.; Contreras, D.S.; Clancy, Y.L.; Lobkovsky, E.B.; Yaghi, O.M.; Dai, S. (2006) A microporous metal-organic framework for gas-chromatographic separation of alkanes. *Angew. Chem., Int. Ed.*, *45* (9): 1390.
5. Langmuir, I. (1918) The adsorption of gases on plane surfaces of glass, mica and platinum. *J. Chem. Soc.*, *40* (9): 1361.
6. Bárcia, P.S.; Silva, J.A.C.; Rodrigues, A.E. (2006) Separation by fixed-bed adsorption of hexane isomers in zeolite BETA pellets. *Ind. Eng. Chem. Res.*, *45*: 4316.
7. Bárcia, P.S.; Silva, J.A.C.; Rodrigues, A.E. (2007) Multicomponent sorption of hexane isomers in zeolite BETA. *AIChE.*, *53* (8): 1970.
8. Villadsen, J.V.; Michelsen, M.L. (1978) *Solution of Differential Equation Models by Polynomial Approximation*; Prentice-Hall: Englewood Cliffs, NJ.
9. Wakao, N.; Funazkri, T. (1978) Effect of fluid dispersion coefficients on particle-to-fluid mass transfer coefficients in packed beds: Correlation of sherwood numbers. *Chem. Eng. Sci.*, *33*: 1375.
10. Cavenati, S.; Grande, C.A.; Rodrigues, A.E. (2006) Separation of $CH_4/CO_2/N_2$ mixtures by layered pressure swing adsorption for upgrade of natural gas. *Chem. Eng. Sci.*, *61*: 3893.
11. Farooq, S.; Ruthven, D.M. (1990) Heat effects in adsorption column dynamics. 2. Experimental validation of the one-dimensional model. *Ind. Eng. Chem. Res.*, *29* (6): 1084.
12. Dwivedi, P.N.; Upadhyay, S.N. (1977) Particle-fluid mass transfer in fixed and fluidized beds. *Ind. Eng. Chem. Process Des. Dev.*, *16* (2): 157.
13. Huang, Y.Y. (1973) Quadrupole interaction of carbon dioxide on silica-alumina surface. *J. Phys. Chem.*, *77* (1): 103.
14. Li, D.; Kaneko, K. (2001) Hydrogen bond-regulated microporous nature of copper complex-assembled microcrytals. *Chemical Physics Letters*, *335*: 50.
15. Bourrelly, S.; Llewellyn, P.L.; Serre, C.; Millange, F.; Loiseau, T.; Férey, G. (2005) Different adsorption behaviors of methane and carbon dioxide in the isotypic nanoporous metal terephthalates MIL-53 and MIL-47. *J. Am. Chem. Soc.*, *127*: 13519.
16. Fletcher, A.J.; Thomas, K.M.; Rosseinsky, M.J. (2005) Flexibility in metal-organic framework materials: Impact on sorption properties. *Journal of Solid State Chemistry*, *178*: 2491.
17. Yang, R.T. (1987) *Gas Separation by Adsorption Processes*; Butterworth: Boston.
18. Llewellyn, P.L.; Bourrelly, S.; Serre, S.; Vimont, A.; Daturi, M.; Hamon, L.; Weireld, G.D.; Chang, J.S.; Hong, D.Y.; Hwang, Y.K.; Jhung, S.H.; Férey, G. High uptakes of CO_2 and CH_4 in mesoporous metal-organic frameworks MIL-100 and MIL-101. *J. Am. Chem. Soc.*, (in press).

19. Papadopoulos, G.K.; Jobic, H.; Theodorou, D.N. (2004) Transport diffusivity of N2 and CO2 in silicalite: coherent quasielastic neutron scattering measurements and molecular dynamics simulations. *J. Phys. Chem. B*, *108*: 12748.
20. Krishna, R.; Baten J.M. (2008) Insights into diffusion of gases in zeolites gained from molecular dynamics simulations. *Microporous and Mesoporous Materials*, *109*: 91.
21. Harlick, P.J.E.; Tezel, F.H. (2002) Adsorption of carbon dioxide, methane, and nitrogen: pure and binary mixture adsorption by ZSM-5 with SiO_2/Al_2O_3 ratio of 30. *Separation Science and Technology*, *37* (1): 33.
22. Barrer, R.M.; Davies, J.A. (1970) Sorption in decationated zeolites. I. Gases in hydrogen-chabazite. *Proceedings of the Royal Society of London. Series A, Mathematical and Physical Sciences*, *320* (1542): 289.
23. Ruthven, D.M. (1984) *Principles of Adsorption and Adsorption Process*; John Wiley & Sons: New York.